ACS APPLIED MATERIALS & INTERFACES

Research Article

www.acsami.org

Understanding the Adsorption Interface of Polyelectrolyte Coating on Redox Active Nanoparticles Using Soft Particle Electrokinetics and Its Biological Activity

Shashank Saraf,[†] Craig J. Neal,[†] Soumen Das,[†] Swetha Barkam,[†] Rameech McCormack,[†] and Sudipta Seal*[,†,‡]

[†]Advanced Materials Processing and Analysis Center (AMPAC), Materials Science Engineering (MSE), University of Central Florida, 4000 Central Florida Boulevard, Orlando, Florida 32816, United States

[‡]NanoScience Technology Center (NSTC), Materials Science Engineering (MSE), University of Central Florida, 4000 Central Florida Boulevard, Orlando, Florida 32816, United States

Supporting Information

ABSTRACT: The application of cerium oxide nanoparticles (CNPs) for therapeutic purposes requires a stable dispersion of nanoparticles in a biological environment. The objective of this study is to tailor the properties of polyelectrolyte coated CNPs as a function of molecular weight to achieve a stable and catalytic active dispersion. The coating of CNPs with polyacrylic acid (PAA) has increased the dispersion stability of CNPs and enhanced the catalytic ability. The stability of PAA coating was analyzed using the change in the Gibbs free energy computed by the Langmuir adsorption model. The adsorption isotherms were determined using soft particle electrokinetics which overcomes the challenges presented by other techniques. The change in Gibbs free energy was highest for CNPs coated with PAA of 250 kg/mol indicating the most stable coating. The change in free energy for PAA of 100 kg/mol coated CNPs was 85% lower than the PAA of 250 kg/mol coated CNPs. This significant difference is caused by the strong adsorption of PAA of 100 kg/mol on CNPs. Catalytic activity of PAA-CNPs is assessed by the catalase enzymatic mimetic activity of nanoparticles. The catalase activity was higher for PAA coated CNPs as compared to bare CNPs which indicated preferential adsorption of hydrogen peroxide induced by coating. This indicates that the catalase activity is also affected by the structure of the coating layer.

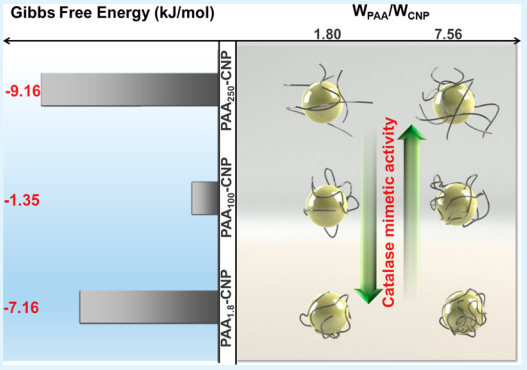

KEYWORDS: *cerium oxide nanoparticles, Gibbs free energy, colloidal dispersion, soft particle electrokinetics, polymer coating, catalase activity*

1. INTRODUCTION

Nanometer-sized cerium oxide particles have potential mechanical, chemical, and biological applications such as in polishing slurries,[1] sensors,[2] catalyst,[3] etc. In recently reported studies, CNPs have known to mimic naturally existing enzymes such as superoxide dismutase (SOD)[4,5] and catalase,[6] thereby posing to be a potential artificial antioxidant.[7−10] Various in vivo and in vitro studies have been performed using CNPs[11] to illustrate successful prevention of tissue damage from radiation,[12−15] laser-induced retinal damage.[16] Some of the other acknowledged applications of CNPs include reduction in chronic inflammation[17,18] and spinal injury,[19,20] promotion of angiogenesis,[8,21,22] and an increase in counts of photoreceptor cells.[23] The underlying mechanism behind the antioxidant property of CNPs is attributed to its ability to modulate its valence states under appropriate redox environment.[12] The catalytic activity can be further enhanced by reducing the size of CNPs.[24] The use of catalytically active CNPs in biological milieu demands a stable dispersion of nanoparticles. Typically the aqueous dispersion of any type of nanoparticles is mainly controlled by its concentration, ionic strength, and pH of the solution.[25−27] The concern of obtaining a stable dispersion of nanoparticles has received considerable attention over the last two decades, and several strategies have been formulated to achieve it. One of the important strategies is the use of polyelectrolytes as a coating agent.[28] They are a class of polymer, where each monomer consists of an electrolyte group that can be ionized by controlling the pH[29] and ionic strength of the solution.[30] The stability of dispersion of polyelectrolyte coated nanoparticles arises from the electrostatic force of repulsion and the steric hindrance generated by the charged coated layer.[31] Polyelectrolytes have been used to stabilize CNPs dispersion in physiological pH where dispersion of bare CNPs undergoes aggregation.[32] Other advantages of using

Received: November 20, 2013
Accepted: March 27, 2014
Published: March 27, 2014

   dx.doi.org/10.1021/am405250g | ACS Appl. Mater. Interfaces 2014, 6, 5472−5482

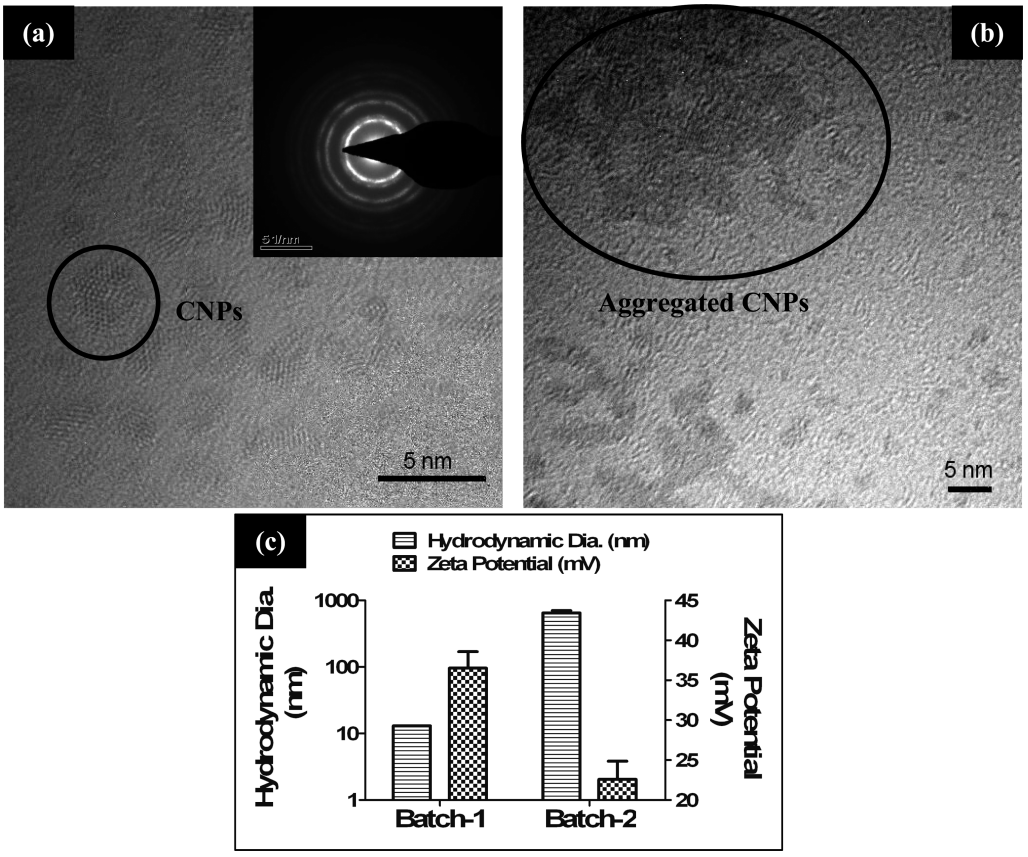

Figure 1. Characterization of CNPs in batch-1 and batch-2 using TEM, SAED, hydrodynamic diameter, and the zeta potential. Parts (a) and (b) show the TEM images of CNPs in batch-1 and batch-2, respectively, depicting the nanoparticles in batch-1 and nanoparticles aggregation in batch-2. The inset of part (a) shows the SAED pattern indicating fluorite crystal structure of CNPs. Part (c) shows the hydrodynamic diameter and the zeta potential of batch-1 and -2. The hydrodynamic diameter increased substantially, while the zeta potential decreased in batch-2.

polyelectrolyte coating on CNPs is that it is to prevent biofouling of nanoparticles[33] and preserve its catalytic nature.[34]

In this study we have selected polyacrylic acid (PAA) which is one of the well-known biocompatible polyelectrolytes which has been studied in multiple in vivo and in vitro systems.[35,36] PAA coated CNPs have demonstrated excellent dispersion in biologically pertinent solutions;[37] however, coating of PAA as a function of different chain lengths is still not fully understood. The chain length of polymer plays an important role in determining the coating stability on nanoparticles.[38] It also affects the interface of the adsorbed polymer which influences the kinetics of reaction of nanoparticles with different substrates.[39] Thereby the tailoring of the PAA coating on CNPs can be achieved by understanding the effect of its chain length on the properties of the coated PAA layer. Generally the polyelectrolyte coating on nanoparticles is facilitated by its adsorption which is in turn influenced by its chain length,[40] size of nanoparticles,[41] and the electrostatic attraction.[42] In this study, the PAA chain length alone was varied keeping the other parameters constant.

Polyelectrolytes of different chain lengths affect the structure of the adsorbed layer on the nanoparticles[40] which governs the volume fraction of adsorbed polymer on them as a function of radial distance. Typically the structure of an adsorbed polymer layer can be classified in three different types: trains, loops, and tails. The polymer segments that are in direct contact with surfaces are defined as trains, polymer segments which connect the trains are called loops, and polymer segments that are only connected to adsorbent surfaces at one end are known as tails. Thus, the surface area of nanoparticles available for interaction with the environment depends on the volume fraction of polyelectrolyte in train, loop, and tail structure which in turn governs the reaction kinetics. Thereby determining the properties of adsorbed layer of PAA-CNPs is of prime importance to fine tune the applications of CNPs.[43]

In previously reported studies, the Ohshima model of soft particle electrokinetics is used to illustrate the behavior of the adsorbed polyelectrolyte layer on nanoparticles in aqueous solution.[44−46] This model uses the electrophoretic mobility of polymer coated nanoparticles to determine the properties of the adsorbed layer. The electrophoretic mobility was obtained for different ratios of amount of PAA over CNPs and fitted in the Ohshima model to acquire the adsorption isotherms. Adsorption isotherms for adsorbed polyelectrolytes on nanoparticles is often fitted using the Langmuir model to obtain Gibbs free energy of adsorption.[43] Thereby using the above mentioned principle the Gibbs free energy of the different molecular weights of PAA adsorption on CNPs are estimated. In this study, CNPs were tuned to be catalase active[9] to access the effect of PAA coating on enzyme mimetic kinetics of CNPs.

2. EXPERIMENTAL SECTION

2.1. CNPs Synthesis. CNPs are synthesized by the thermohydrolysis route by using the concept as demonstrated in the patent.[47] The procedure involves dissolution of ceric(IV) ammonium nitrate in water to form 1 M of Ce^{+4} ions. The solution mixture was then heated at 100 °C under refluxing conditions and stirred at 100 rpm. The

dx.doi.org/10.1021/am405250g | ACS Appl. Mater. Interfaces 2014, 6, 5472−5482

reaction mixture was allowed to equilibrate before adding 1 normality (N) of NH_4OH. Upon the drop-wise addition of NH_4OH a purple color precipitate started to form which indicates the hydrolysis reaction of ceric(IV) ammonium nitrate. The reaction was left for heating for 24 h to obtain a dispersion of CNPs.

2.2. PAA Coating on CNPs. PAA of 1.8, 100, and 250 kg/mol molecular weight are used to coat CNPs. PAA was coated on CNPs by using the procedure listed in ref 37 with slight modifications. Multiple samples of PAA coated CNPs are prepared in acidic pH with a varying ratio of W_{PAA}/W_{CNP} from 1.89 to 7.56. The acidic media prevented CNPs to aggregate and imparted a positive charge on CNPs which in turn get electrostatic attraction from an electron lone pair in a carboxyl group of the PAA polymer. The mixture containing PAA and CNPs was left in an isothermal bath for 1 h which was maintained at 298 K for 1 h. PAA coated CNPs are removed by centrifugation and then redispersed in a solution which was buffered at pH 10.

2.3. Catalase Activity Measurements. Catalase activity of samples was measured using an Amplex Red Hydrogen Peroxide/Peroxidase Assay Kit obtained from Invitrogen. The kit contains Amplex red reagent (10-acetyl-3,7-dihydroxyphenoxazine) which reacts with hydrogen peroxide (H_2O_2) in the presence of horseradish peroxidase (HRP). The product formed in this reaction is resorufin which was detected using UV−visible spectroscopy having absorption maxima at a wavelength of 571 nm. PAA-CNPs were suspended in distilled water; therefore, distilled water (>18 MΩhms) was used as a control. 10 μL of 1 mM CNPs were used for the catalase activity estimation.

2.4. Cell Viability. The cytotoxicity studies of CNPs and PAA coated CNPs were performed on the MG-63 cell line using the MTT (3-(4,5-dimethylthiazol-2-yl)-2,5-diphenyltetrazolium bromide) assay. The MTT dye reduces to a purple color formazon in the presence of mitochondrial dehydrogenases, indicating the presence of living cells. The experimental procedure includes the incubation of different concentrations (0.1−100 μM) of PAA-CNPs at 5.03 W_{PAA}/W_{CNPs} for 12 h with cell culture. A MTT solution of concentration 0.5 mg/mL was then added to the cell culture and incubated for 3.5 h. The formazon produced is then detected spectrophotometrically at a wavelength of 570 nm.

2.5. Intercellular ROS Estimation. $3-5 \times 10^3$ Cells were seeded in 96 wells plate for fluorescence estimation. Cells were then treated with different concentrations (0.1, 0.5, 1, 10, and 100 μM) and different types ($PAA_{1.8}$-CNPs, PAA_{100}-CNPs, and PAA_{250}-CNPs) of PAA-CNPs at 5.03 W_{PAA}/W_{CNPs} in triplicates and incubated for 12 h. Then cells were washed, and 50 μM final concentration of H_2-DCF-DA was added to cells and incubated for 30 min in an incubator. Next, cells were washed three times with saline, and fluorescence intensities were measured using a plate-reader. Florescence intensities were plotted as mean and standard error.

3. RESULTS AND DISCUSSION

3.1. Structural Properties of CNPs. A detailed characterization of CNPs was performed using transmission electron microscopy (TEM), dynamic light scattering (DLS), and X-ray photoelectron spectroscopy (XPS) to determine size, crystal structure, surface potential, and surface chemistry respectively of the nanoparticles. The concentration of cerium oxide in as-synthesized CNPs (termed as batch-1) is 28 mM which was determined using gravimetric analysis with pH 1.48. Another batch of CNPs (batch-2) was prepared by diluting batch-1 to 1000 times, keeping the pH constant. The reduced concentration of cerium oxide was pertinent to therapeutic applications. Visual observation of batch-1 indicated a stable dispersion for extended periods of time; while batch-2 showed aggregation within 24 h of storage. The TEM images of CNPs corresponding to batch-1 and batch-2 are shown in Figure 1a and 1b, respectively. Batch-1 CNPs (Figure 1a) were well dispersed with an average particle size of ~5 ± 0.7 nm which was computed statistically for over 50 data points. Batch-2 (Figure1b) on the other hand exhibited large aggregates with an irregular size, indicating unstable dispersion. The selected area electron diffraction (SAED) pattern (inset of Figure 1a) confirms the fluorite crystal structure of cerium oxide. Hydrodynamic diameter (HD) of batch-1 and batch-2 are ~10 nm and ~700 nm respectively that were measured using DLS (Figure 1c). The hydrodynamic diameter of CNPs in batch-1 obtained from DLS was slightly bigger as determined from TEM image analysis. This difference in diameter arises from the adsorption of nitrate ions on CNPs and the associated double layer of CNPs dispersed in aqueous solution. The size of CNPs in batch-2 obtained from both techniques indicated a state of aggregation. The zeta potential of CNPs in batch-1 is 36 mV as compared to 23 mV upon dilution in batch-2 (Figure 1c). The conductivity of the batch-1 solution is 3.15 mS/cm which increased to 37.6 mS/cm in batch-2 solution. Conductivity is a linear function of the ionic concentration of solution, indicating more ionic concentration in batch-2 as compared to batch-1. The results suggest that the aggregation of 1000 times diluted CNPs are caused by fluctuations in ionic concentration which shows the extreme susceptibility of CNPs towards the change in ionic strength of dispersion media. The aggregation in batch-2 alters the ratio of oxidation states of CNPs which is discussed in later sections. Polyacrylic acid coated CNPs (PAA-CNPs) are found to prevent this aggregation and still preserve the surface chemistry of CNPs as discussed in the sections below. The procedure for PAA coating on CNPs is described in detail in the experimental technique.

3.1.1. Morphological Characterization of PAA-CNPs. In the study, CNPs are coated with different chain lengths of PAA which was achieved by using different molecular weight (MW) of PAA. The PAA was coated on CNPs using a chemical route as mentioned by Sehgal et al.[37] with slight modifications. The detailed coating procedure is outlined in the Experimental Section. The PAA coating was accomplished by its adsorption on the surface of CNPs, which are dispersed in acidic aqueous solution. The adsorption of PAA was influenced by the electrostatic attraction between the positively charged nanoparticles and the polymer which is uncharged. The PAA coated CNPs were removed from the solution by centrifugation and collected at the bottom of the centrifuge tubes in the form of pellets, which were then redispersed in aqueous solution maintained at pH 10. At this pH the carboxyl group on PAA gets ionized as PAA has a pK_a value close to 4.5[48] which is independent of its chain length. Thereby, PAA-CNPs acquired a negative charge and form a stable dispersion resulting from electrostatic repulsion between them. The synthesized PAA-CNPs are characterized to analyze the size and structure of adsorbed polymer layer. The molecular weights of PAA which are selected to coat CNPs were 1.8, 100, and 250 kg/mol, which differ widely in their chain lengths and denoted by following notations: $PAA_{1.8}$, PAA_{100}, and PAA_{250}. Theoretically the chain lengths of PAA have shown to be computed from the mean-field theory as a function of molecular weight. The chain length of PAA is given by the root mean square (rms) of end-to-end distance of a PAA chain which is illustrated using the following relationship[49]

$$\langle R_o^2 \rangle = C_\infty l^2 N \quad (1)$$

where C_∞ is the characteristic ratio, l is the length of a monomer of PAA which is taken to be 0.256 nm,[49] and N is the

number of monomers in a PAA chain. The value of C_∞ is determined from the mean-field theory simulations. The estimated value of C_∞ is about 19 which is valid when the ionic concentration of PAA-CNPs solutions is close to 0.01 M corresponding to the symmetrical electrolyte.[49] The calculated lengths of PAA in aqueous solution maintained at pH 10 are used to obtain the theoretical diameter of PAA-CNPs.

Multiple samples of PAA-CNPs were prepared for each molecular weight of PAA, by varying the weight fraction (W_{PAA}/W_{CNPs}) from 1.89 to 7.56 in the adsorbing mixture. The effect of increasing PAA weight fraction results in an increment of its adsorption density on CNPs. DLS was used to determine the hydrodynamic diameter (HD) of PAA-CNPs as a function of the molecular weights. HD was plotted as a function of W_{PAA}/W_{CNPs} for all the MW PAA coated CNPs (Figure 2a).

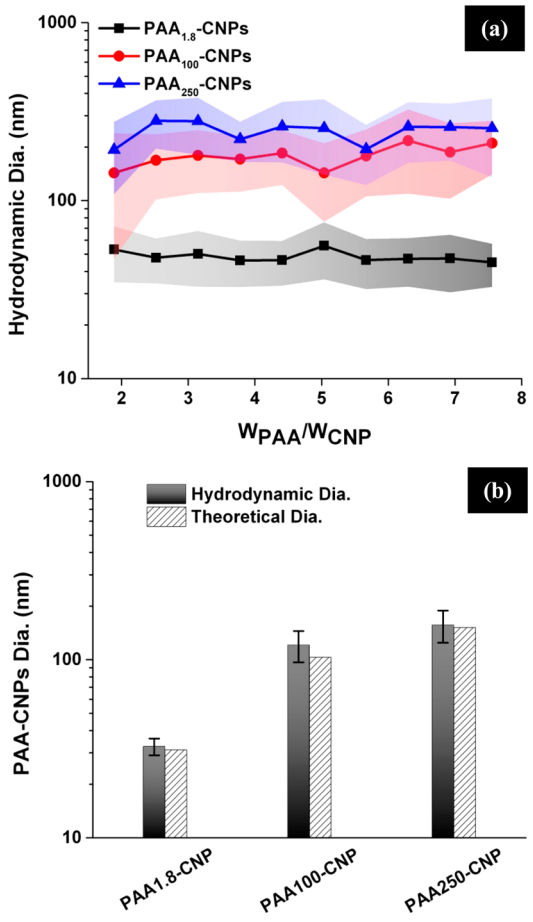

Figure 2. Part (a) shows the hydrodynamic diameter of PAA coated CNPs as a function W_{PAA}/W_{CNP} which depicts the similar size of nanoparticles belonging to the same molecular weight over the PAA weight fraction. Part (b) shows a comparison of sizes obtained experimentally using DLS and theoretically using mean field theory. It shows the similar size from both methods indicating the core-shell morphology for PAA-CNPs.

Evidently HD of PAA-CNPs belonging to the same MW is nearly constant in the aforementioned range of weight fraction of PAA used for the adsorption experiment. An average size was then determined for PAA-CNPs corresponding to their MW (Figure2b). The experimentally determined size of PAA-CNPs was compared to that of the theoretical size which was calculated using the mean-field theory. Previous studies based on the mean field theory simulations have concluded that the length of an adsorbed polyelectrolyte extends up to the twice its rms end-to-end length (R_o)[40] which was used to calculate the theoretical size of PAA-CNPs as a function of the molecular weight of PAA which is mentioned below

$$D = 4R_o + D_{CNP} \quad (2)$$

where D is the theoretical diameter, R_o is the rms length of PAA, and D_{CNP} is the diameter of CNPs as determined using TEM. The calculated theoretical size of PAA-CNPs is shown in Table 1 and is nearly similar to the experimental HD of PAA-CNPs particles (Figure 2b) indicating that the particles are not bridged to each other. Thereby it can be interpreted that the PAA-CNPs nanoparticles have core-shell morphology with CNPs as the core and PAA adsorbed layer as the shell. The coating thickness (δ) was obtained by deducting the radius of CNPs from the hydrodynamic radius of PAA-CNPs.

3.1.2. Preservation of Surface Chemistry of CNPs. The antioxidant properties of CNPs are primarily governed by its surface chemistry which was determined using the relative concentration of cerium in +3 and +4 valence states.[34] The relative concentration can be quantified from UV−visible spectrophotometry and XPS. In a typical UV−vis spectrum of CNPs having mixed valence states, the absorption maxima close to 298 and 260 nm corresponds to +4 and +3 valence states, respectively.[34] The intensity of absorption maxima is directly proportional to the concentration of the corresponding species as stated by Beer-Lambert's law ($A = \epsilon cl$, where ϵ is the molar absorptivity, c is the concentration, and l is the path length). The UV−vis spectra of CNPs in batch-1, batch-2, and PAA-CNPs (Figure 3a) depicted the local absorption maxima at wavelengths 298 and 260 nm indicating the presence of mixed valence states in CNPs. The spectrum of batch-2 CNPs exhibited a decrease in the intensity of absorption at 260 nm and an increase at 298 nm as compared to that of batch-1 suggesting partial transformation of cerium in the +3 to the +4 state. Thus, aggregation induced by reduction in the zeta potential in batch-2 altered the surface chemistry of CNPs. On the other hand, the UV−vis spectrum of PAA-CNPs is quite similar to that of CNPs in batch-1 signifying the preservation of the surface chemistry due to coating of PAA. The surface chemistry of CNPs in batch-1 was quantified using XPS. The XPS spectrum of Ce(3d) is marked by its characteristic peaks of both valence states of Ce (+3 and +4) (Figure 3b). Relative concentration of Ce in the +3 over the +4 valence state is calculated from the deconvoluted spectra as shown in Figure 3b (dotted lines). The deconvoluted spectrum consists of peaks contribution from both valence states as well as from the multiple d-splitting.[50] The ratio of Ce in the +3 over the +4 state is estimated to be 0.25, which was calculated using the summation of the integrated area under the corresponding deconvoluted peak. The detailed procedure of obtaining Ce(+3)/Ce(+4) ratio is listed in the Supporting Information. Thereby in batch-1 Ce in the +4 state is greater in quantity than in the +3 state. It has been previously established that CNPs with more +4 state are known to exhibit catalase activity.[17] Due to the presence of polymer in PAA-CNPs, the signal from Ce was very weak to be analyzed in XPS for comparison.

3.2. Determination of Adsorption Isotherms. The adsorption of PAA on CNPs can be defined by the number of moles of PAA adhered on a single CNP. Polymer adsorption on nanoparticles is often determined by using solution depletion analysis.[51] In this technique free polymer in a supernatant is analyzed which is separated from polymer

Table 1. Hydrodynamic Diameter, Theoretical Diameter, Electrophoretic Softness, and Gibbs Free Energy of PAA-CNPs as a Function of Molecular Weight

name	hydrodynamic diameter (nm)	theoretical diameter (R_{CNP} + 4R_o) (nm)	electrophoretic softness (nm^{-1})	Gibbs free energy (J/mol)	coating thickness (δ) (nm)
$PAA_{1.8}$-CNPs	32.55 ± 3.478	31.16	4.49	−7160.39	19.55
PAA_{100}-CNPs	120.80 ± 24.247	103.18	53.66	−1352.65	107.80
PAA_{250}-CNPs	156.60 ± 31.985	151.50	38.04	−9162.83	143.60

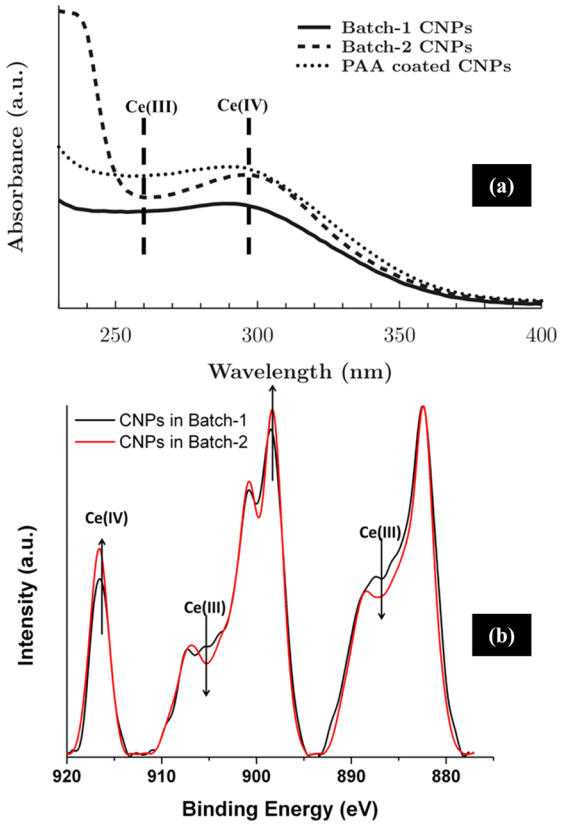

Figure 3. Characterization of surface chemistry (i.e. Ce(+3)/Ce(+4)) using UV−vis and XPS spectrum of CNPs in batch-1 and batch-2 and PAA-CNPs. Part (a) depicts the UV−vis spectra illustrating the mixed valence state in CNPs. The loss of intensity around 298 nm in CNPs of batch-2 indicating change in surface chemistry while PAA-CNPs exhibiting a similar spectrum as CNPs in batch-1 indicating preservation of surface chemistry. Part (b) depicts the XPS spectrum of Ce(3d) for CNPs in batch-1 and -2 which shows the peak contribution from both oxidation states. The reduced intensity of Ce(+3) peaks and increased intensity of Ce(+4) of CNPs in batch-2 as compared to batch-1 indicates the same trend as depicted in UV−vis.

adsorbed nanoparticles using centrifugation. However, particle separation using a centrifuge may not completely remove polyelectrolyte coated nanoparticles from free polymer leading to incorrect analysis. Thereby we have adopted a novel technique to determine adsorption isotherm by measuring electrophoretic mobility (EM) which is related to the polymer adsorbed on nanoparticle. EM is defined as the terminal velocity of dispersed particles under the influence of an applied electric field. It is affected by the charge density on the particles arising from the negatively charged PAA layer and the ionic strength of the solution. The amount of charge density is attributed to the number of −COOH groups in the adsorbed polymer. The EM of PAA-CNPs was measured at pH 10, where PAA was completely ionized indicating unit charge per monomer of PAA. The ionic strength results in lower EM due to increased shielding of the charged polymer layer. The ionic strength is directly related to the conductivity of a solution. Both EM and conductivity are recorded as a function of W_{PAA}/W_{CNP} which are used in the Ohshima model to compute the number charge density of the polyelectrolyte charge originating from a carboxylic group (−COOH).

3.2.1. Electrophoresis Model of Soft Particles. The zeta potential of particles can be derived from their electrophoretic mobility by using the Smoluchowski theory, which assumes a perfect rigid nature of the particle. Ohshima et al.[46] applied corrections to the existing model to study the penetration of fluid inside porous particles which include illustrations of polymer coated nanoparticles. The derived expression of electrophoretic mobility depends on several parameters such as charge density of the polyelectrolyte layer, ionic concentration of solvent, and the reciprocal of λ where $1/\lambda$ is known as electrophoretic softness. The following expression was used to compute the electrophoretic mobility (EM)

$$\mu = \frac{\varepsilon_r \varepsilon_o}{\eta} \frac{\left(\frac{\varphi_o}{\kappa_m} + \frac{\varphi_{DON}}{\lambda}\right)}{\left(\frac{1}{\kappa_m} + \frac{1}{\lambda}\right)} f\left(\frac{b}{a}\right) + \frac{ZeN}{\eta\lambda^2} \quad (3)$$

where ε_r is the relative permittivity of solvent, ε_o is the permittivity of free space, e is the elementary charge, and η is the viscosity of solvent. The valence and number density of charge is denoted by Z and N, respectively, present on polyelectrolyte coated layer. The zeta potential and the Donnan potential are represented by φ_o and φ_{DON}, respectively. κ_m is the effective Debye-Huckel parameter of the surface polyelectrolyte layer. The radius of polyelectrolyte coated nanoparticle is represented by b, and the radius of the nanoparticle is denoted by a. The above mentioned parameters are presented below in detail.

$$\varphi_{DON} = \frac{kT}{ze}\sinh^{-1}\left(\frac{ZN}{2zn}\right) \quad (4)$$

$$\varphi_o = \varphi_{DON} - \frac{kT}{ze}\tanh\left(\frac{Ze\varphi_{DON}}{2kT}\right) \quad (5)$$

$$\kappa_m = \kappa\left[\cosh\left(\frac{ze\phi_{DON}}{kT}\right)\right]^{1/2} \quad (6)$$

$$\kappa = 4314940^*\left(\frac{I}{\varepsilon_r\varepsilon_o RT}\right)^{1/2} \quad (7)$$

$$f\left(\frac{b}{a}\right) = \frac{2}{3}\left(1 + \frac{a^3}{2b^3}\right) \quad (8)$$

where k is the Boltzmann constant, T is the temperature at which electrophoretic mobility is measured, and z is the valence of electrolyte. The ionic concentration of the solution is

denoted by I. The Debye-Huckel parameter of the solution is denoted by κ.

3.2.2. Parameters for Soft Particle Electrophoretic Mobility Modeling. Electrophoretic softness parameter i.e. $1/\lambda$ can be determined experimentally by the procedure mentioned in ref 44. It was obtained by fitting EM as a function of ionic concentration of the solvent in eq 3. The experimentally measured values of EM v/s ionic concentration for $PAA_{1.8}$-CNPs, PAA_{100}-CNPs, and PAA_{250}-CNPs are displayed in Figure 4a, 4b, and 4c, respectively. In the same figure the black line

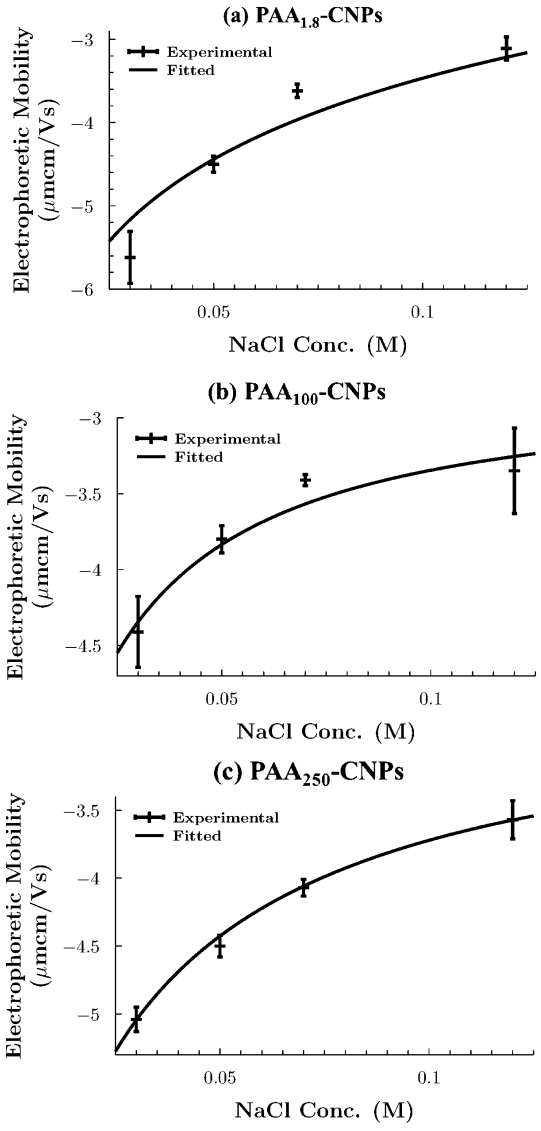

Figure 4. Electrophoretic mobility of PAA-CNPs as a function of sodium chloride concentration which is determined using Malvern's Zetasizer nano series instrument. Parts (a), (b), and (c) show the experimental data and fitted data (line) for $PAA_{1.8}$-CNPs, PAA_{100}-CNPs, and PAA_{250}-CNPs, respectively.

represents the nonlinear fitting of data points using the Ohshima model. The values of $1/\lambda$ obtained from the nonlinear fitting of data are summarized in Table 1 for PAA-CNPs as a function of the molecular weights of PAA. This parameter is largest for PAA_{100}-CNPs which indicates the highest degree of softness in PAA coating resulting from dense packing of PAA closer to the CNPs surface while sparse packing away from CNPs surface. As previously stated that the HD of PAA-CNPs does not vary with W_{PAA}/W_{CNP}, thus indicating the distance between the particle core and the slipping plane would also remain unchanged. Thereby, it can be assumed that the softness parameter would be the same for PAA-CNPs of the same molecular weight having different W_{PAA}/W_{CNP}.

3.2.3. Adsorption Isotherms. The adsorption behavior of PAA on a nanoparticle was determined indirectly by obtaining EM of nanoparticles as a function of W_{PAA}/W_{CNP}. Adsorption of PAA is varied by modulating W_{PAA}/W_{CNP} from 1.89 to 7.56 where particle bridging is not prominent. Figure 5a, 5b, and 5c (left) depicts the EM of PAA-CNPs and conductivity as a function of W_{PAA}/W_{CNP}. As previously stated, EM of nanoparticles is a nonlinear function of charge density of the shell, ionic strength of solution, and electrophoretic softness parameter. The ionic strength was determined from the conductivity of the solution, thereby a calibration curve was generated for conductivity as a function of ionic strength to calculate an unknown ionic strength. The detailed procedure of the same is elaborated in the Supporting Information. Computed ionic strength, softness parameter, and EM are substituted in the Ohshima model to find the charge density of PAA-CNPs. This charge density in PAA-CNPs originates from the ionized carboxylic groups −COOH present in every monomer which increases proportionately with the PAA adsorption. Each monomer contributes one unit charge coming from the −COOH group. The polymer adsorbed on CNPs surface was derived from calculated charge density

$$\Gamma = N^* \frac{(D_{CNP} + 2\delta)^3}{(D_{CNP})^2} * 72 \tag{9}$$

where Γ is the adsorption density of PAA on CNPs. Using the above theory, absorption curves are thus plotted as a function of −COOH concentration in the adsorbing mixture as shown in Figure 5a, 5b, and 5c (right). The x-axis represents the equilibrium concentration of −COOH moieties. In this concentration regime of PAA coated CNPs, nanoparticles have a core-shell type of morphology which indicates the EM of nanoparticles corresponds to the adsorption behavior of a nanoparticle. The calculated adsorption isotherms indicated a Langmuir type of adsorption. PAA_{100}-CNPs exhibited the highest adsorption density indicating preferential adsorption of this molecular weight on CNPs as compared to other MW of PAA.

3.3. Gibbs Free Energy of PAA Adsorption on CNPs. In previous studies, competitive adsorption between polymers differing in chain lengths reported that higher molecular weight polymer exhibits more stable coating in terms of overall reduction in the Gibbs free energy.[38] The reason was attributed to the low entropy loss in higher molecular weights of PAA adsorbed on surface. However, the kinetics of polymer adsorption favored lower molecular weight PAA, though in the case of an extended period of time the higher molecular weight of PAA replaces the lower molecular weight PAA.[38] Thereby determining Gibbs free energy will determine the long term stability of the coating. Gibbs free energy of PAA adsorption on CNPs was determined by fitting adsorption curves according to the Langmuir adsorption model. The Langmuir model for adsorption assumes that the adsorbate offers infinite sites of adsorption with equal probability.[52] The Langmuir equation is given by

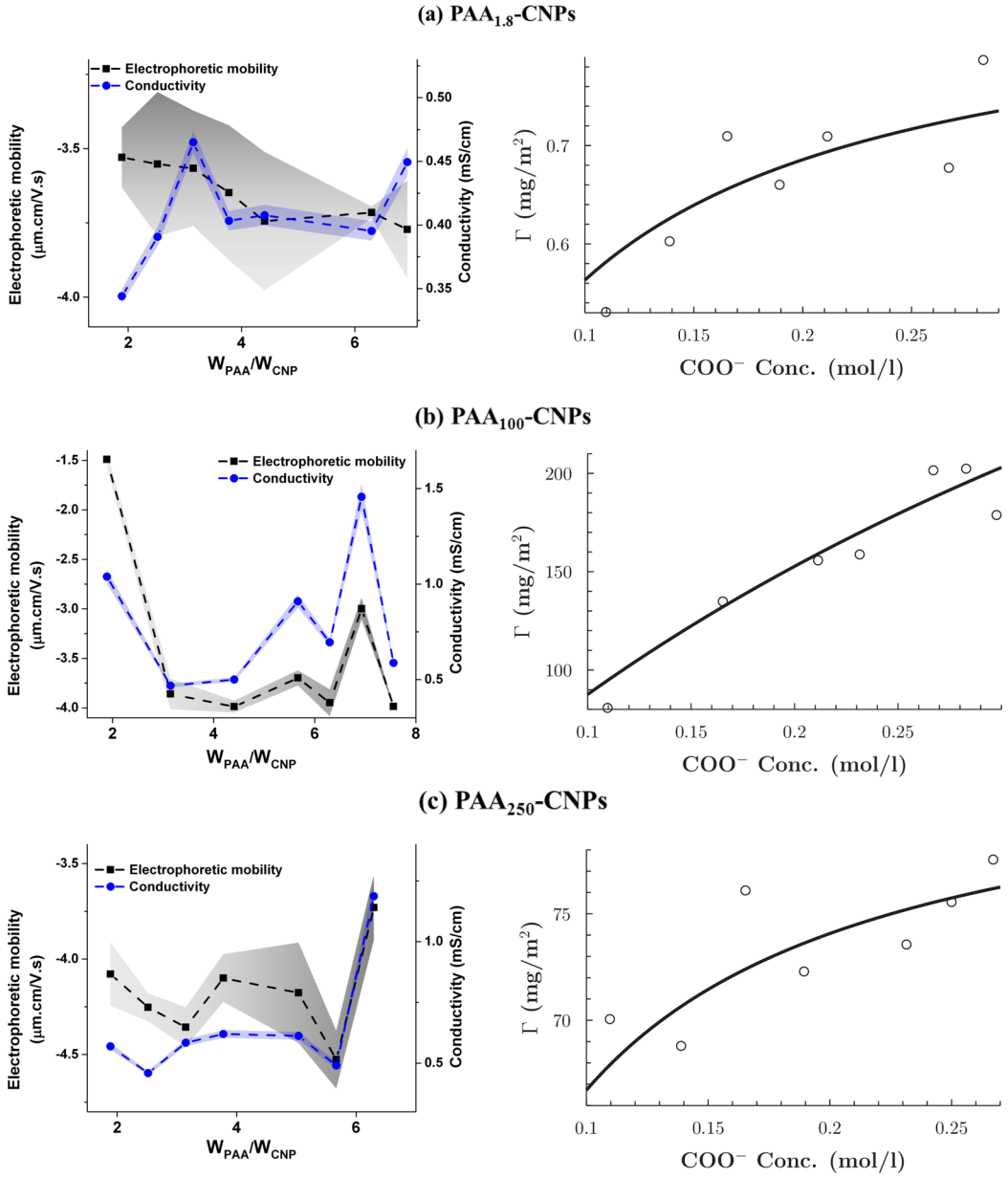

Figure 5. Parts (a), (b), and (c) on the left side show the electrophoretic mobility and conductivity of PAA-CNPs as a function W_{PAA}/W_{CNP} which served as raw data points in soft particle electrokinetics model for $PAA_{1.8}$-CNPs, PAA_{100}-CNPs, and PAA_{250}-CNPs, respectively. Parts (a), (b), and (c) on the right side show the adsorption isotherms (open circles) computed using this model for PAA-CNPs in the same order. The adsorption isotherms were fitted with the Langmuir isotherm model depicted as a black line.

$$\Gamma = \Gamma_{max}\left(\frac{K_{abs}n}{1 + K_{abs}n}\right) \quad (10)$$

where Γ_{max} is the saturation adsorption density of PAA on CNPs. K_{abs} is the chemical equilibrium constant for PAA adsorption on CNPs, and n is the equilibrium concentration of −COOH in the adsorbing mixture. The value of K_{abs} is obtained for all three molecular weights of PAA coated CNPs by fitting the adsorption isotherm as shown in Figure 5a, 5b, and 5c, in the Langmuir model. The Gibbs free energy is calculated from K_{abs} by the following thermodynamic relationship

$$\Delta G_o = -RT \ln(K_{abs}) \quad (11)$$

where R is the gas constant, and T is the temperature of the solution. ΔG_o is the standard Gibbs free energy of PAA adsorption on CNPs in joules per mole. The calculated change in Gibbs free energy is shown in Table 1. According to the obtained values, PAA_{250}-CNPs have the highest change in Gibbs free energy, followed by $PAA_{1.8}$-CNPs. PAA_{100}-CNPs exhibited the lowest change in free energy indicating the least stable coating. Thereby PAA_{250}-CNPs form the most stable coating. The deviation in Gibbs free energy of PAA_{100}-CNPs is caused by the strong adsorption of PAA chains closer to the CNPs surface. As previously mentioned the adsorbed layer structure in PAA_{100}-CNPs consists of strongly adhered PAA chains indicating more volume fraction of polymer close to the surface. This leads to loss in mobility of chains resulting in a high entropic loss of PAA_{100} chains after its adsorption on CNPs which effectively lowers the free energy. The results

dx.doi.org/10.1021/am405250g | ACS Appl. Mater. Interfaces 2014, 6, 5472−5482

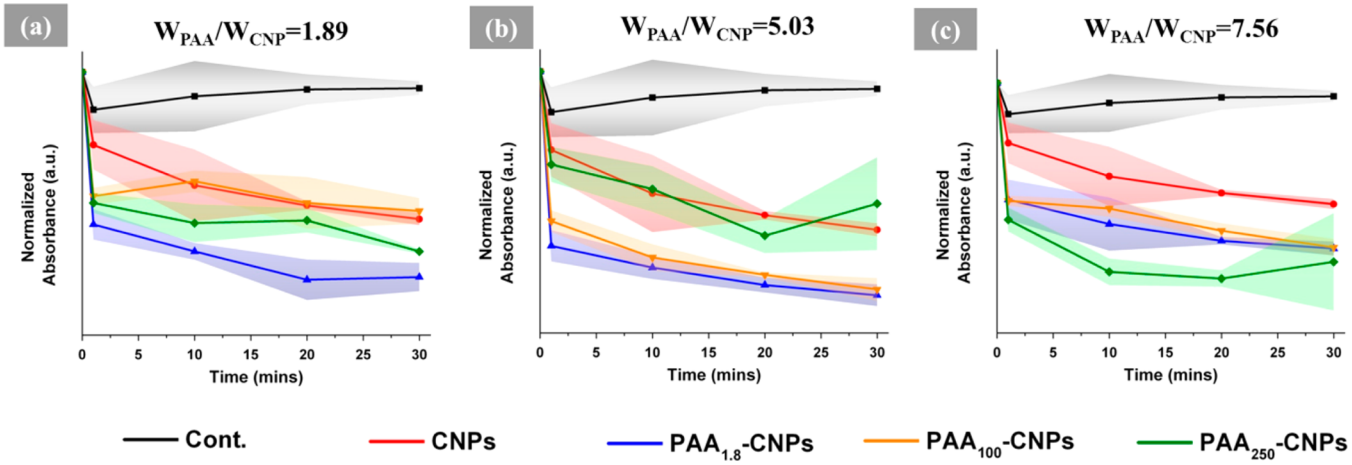

Figure 6. Catalase mimetic activity of PAA-CNPs as a function of W_{PAA}/W_{CNP}. Parts (a), (b), and (c) show the activity for W_{PAA}/W_{CNP} at 1.89, 5.03, and 7.56, respectively.

suggest the preferential adsorption of PAA_{100} over the other molecular weights on CNPs.

3.4. Catalase Activity of PAA-CNPs as a Function of PAA Chain Length. Catalytic properties of CNPs are dependent on its surface chemistry. Previously, we have shown that CNPs having more +4 valence states are catalase active and more +3 valence states are SOD active.[17] CNPs used in this study are specifically tuned to exhibit catalase activity by having more +4 states as compared to +3 on the CNPs surface. The catalase activity of PAA coated CNPs has not been studied as a function of the amount of adsorbed polymer and chain length. The mechanism behind catalase activity is the disproportionation reaction of hydrogen peroxide with the redox active sites present in CNPs. The catalytic activity may decrease after PAA adsorption as many of these sites are blocked by CNP and PAA linkage and the steric hindrance from the adsorbed layer. On the other hand, the catalase activity might also increase if PAA adsorbed CNPs promote preferential bonding between hydrogen peroxide and CNPs. Thus, the structure of the adsorbed PAA layer such as volume fraction of PAA present in train, loop, and tail will play an important role in governing the catalytic activity.

The catalase activity of PAA-CNPs was determined using a catalase kit and plotted as a function of W_{PAA}/W_{CNP} for all molecular weight of PAA used for coating CNPs (Figure 6a, 6b, and 6c). The control sample used in the experiment is catalase inactive; the more deviation from control samples signifies higher catalase activity. The control sample has the maximum absorbance of the dye due to scavenging of H_2O_2 entirely by the amplex red reagent. The amount of H_2O_2 reacting with reagent decreases in the presence of CNPs resulting in the lower absorbance of the dye as CNPs themselves scavenge H_2O_2. It is evident that all PAA-CNPs have higher catalytic activity than bare CNPs. At W_{PAA}/W_{CNP} = 1.89, $PAA_{1.8}$-CNPs has the highest catalytic activity, and PAA_{100} has the lowest, and at W_{PAA}/W_{CNP} = 7.56, PAA_{250} has the highest catalytic activity. Based on these experimental results it can be inferred that peroxide has preferential adsorption on PAA adsorbed CNPs. The preferential adsorption leads to an increased catalytic activity. However, at a higher adsorption density of PAA, the steric hindrance from adsorbed layer is producing resistance for the inward diffusion of peroxide species. PAA_{100}-CNPs have a higher amount of polymer adsorbed as compared to other molecular weights of PAA with an increased catalytic activity. This corresponds to the strong adsorption of PAA_{100} on the surface leading to the decrease in catalytic activity as compared to other molecular weights.

3.5. Biocompatibility of PAA-CNPs. Before considering any nanoparticles for medicinal applications such as drug delivery tools or therapeutic applications, it requires a biocompatibility test. In this study we tested if different molecular weight PAA-CNPs have any severe adverse effects on cells using an in vitro cell culture model. We chose the MG63 cell line for this study due to the fact that the antioxidant activity of PAA-CNPs can be explored in preparing scaffold for tissue/bone regeneration. Cnps can provide strength to hard tissue scaffold as well as the scavenging property can support cell growth by minimizing inflammation. The dosage of particles was taken in the concentration range pertinent to the biological experiment. The cell proliferation results are shown in Figure 7a, and it can be clearly observed that PAA-CNPs exhibits biocompatibility for concentrations less than 100 μm of cerium oxide. Thus, PAA-CNPs did not have any adverse effects on the MG-63 cell line. It is important to note that a normal primary cell line would be a better choice to test nanoparticles toxicity. In future studies the toxicological effect of PAA-CNPs should be explored in a normal primary cell line to draw a solid conclusion. Though particles have no adverse effect on cell viabilities, it would still induce oxidative stress and induce cell membrane/DNA damage. Therefore, we tested reactive oxygen species concentration in PAA-CNPs treated cells, by using 5-(and-6)-chloromethyl-2′,7′-dichlorodihydro-fluorescein (H_2-DCF-DA). Figure 7b shows intracellular ROS generation for different PAA-CNPs at different concentrations. Significant differences in ROS generation were observed when treated with different PAA-CNPs. $PAA_{1.8}$-CNPs did not show any ROS generation in the concentration range tested (0.1–100 μm) as compared to untreated cells. PAA_{100}-CNPs did not show any difference in intracellular ROS up to 10 μm final concentration; at higher concentration (100 μm) it showed a slight increase in ROS generation. However, PAA_{250}-CNPs molecular weight coated CNPs showed a significant increase in intracellular ROS generation in a concentration dependent manner. These results indicate that the size of nanoparticles and the stability of polymer coating plays an important role in cell interaction and toxicity. $PAA_{1.8}$-CNPs nanoparticles owing

dx.doi.org/10.1021/am405250g | ACS Appl. Mater. Interfaces 2014, 6, 5472–5482

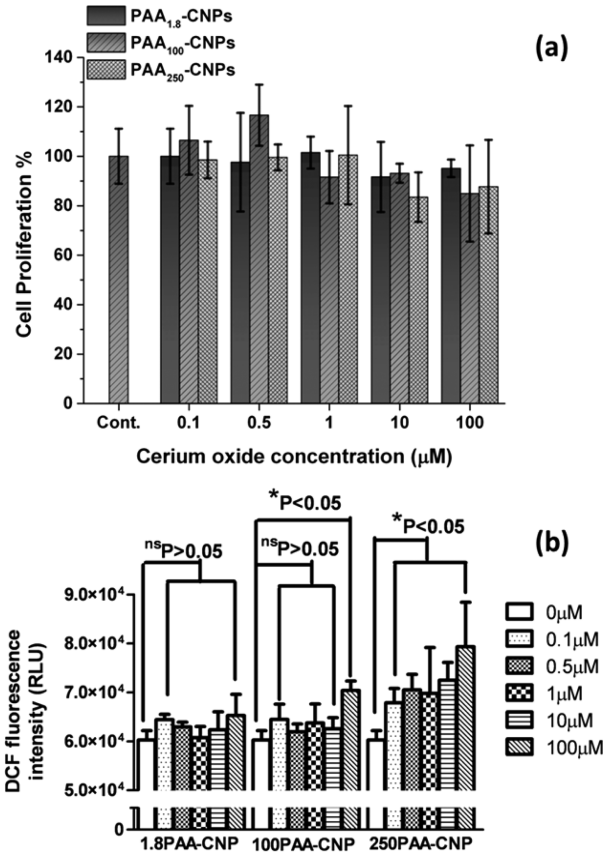

Figure 7. MG-63 cells viability after incubation with PAA-CNPs to determine the biocompatibility of PAA-CNPs. Part (a) It is evident that there is no significant difference in the cell proliferation with the increase in concentration of CNPs coated by different molecular weights. Part (b) A different amount of ROS generation was observed by different PAA-CNPs. Lower concentration ≤10 μM $PAA_{1.8}$-CNPs and PAA_{100}-CNPs did not show any significant different ROS generation. However, PAA_{250}-CNPs at all concentrations tested and ≥100 μM concentration for PAA_{100}-CNPs showed a significant increase in ROS generation compared to untreated cells.

to the lowest hydrodynamic radius showed minimum or no adverse effect on MG-63 cells. However, PAA_{250}-CNPs nanoparticles observed to induce the highest amount of ROS generation may be due to the bigger size of the nanoparticles. The correlation of stability of polymer coating with toxicity was not observed.

4. CONCLUSION

In summary, we have analyzed the critical factors for PAA coated CNPs dispersion for therapeutics which spans from the dispersion stability, bioactivity, and biocompatibility. The stability of bare CNPs dispersion was found to be extremely susceptible to ionic concentration exhibiting aggregation in 1000 times diluted solution. On the other hand, PAA coated CNPs successfully preserved the dispersion stability and surface chemistry of CNPs. The Ohshima model was applied to compute the adsorption isotherm from the electrophoretic mobility of these particles which was modulated by the charge density indicative of the amount of adsorbed PAA. Additionally it was found that the PAA-CNPs were forming a core-shell structure indicating the adsorption isotherm determined from this model is characteristic of single CNP. The standard Gibbs free energy of PAA adsorption on CNPs was determined using the Langmuir adsorption isotherm fitting to the obtained adsorption isotherms. Based on free energy change PAA_{250}-CNPs formed the most stable coating and PAA_{100}-CNPs formed the least stable coating. The structure of the adsorbed PAA layer in the case of PAA_{100} exhibited the highest adsorption density which leads to the lowest change in free energy of adsorption.

The catalase mimetic activity of PAA-CNPs increased in comparison with bare CNPs indicating the increase in disproportionation of hydrogen peroxide by CNPs due to the PAA coating. The catalase mimetic activity for PAA-CNPs also indicated that it was modulated by two contradicting factors: the surface concentration of PAA and the steric repulsion from PAA coating. PAA-CNPs did not cause any adverse cytotoxicity effect and exhibited biocompatibility as obtained from a cell viability experiment. This study can be applied to a wide spectrum of nanoparticles for catalytic applications as well as their long term storage. In conclusion, we have shown the use of correlation between the adsorption thermodynamics of polymer coated nanoparticles and soft particles kinetics to study the intricate interaction of polymers with the physiochemical properties of nanoparticles.

■ ASSOCIATED CONTENT

Supporting Information

Information on materials, characterization techniques, and conductivity calibration curve. This material is available free of charge via the Internet at http://pubs.acs.org.

■ AUTHOR INFORMATION

Corresponding Author

*E-mail: Sudipta.Seal@ucf.edu.

Author Contributions

Craig J. Neal and Rameech McCormack are undergraduate students at the University of Central Florida.

Notes

The authors declare no competing financial interest.

■ ACKNOWLEDGMENTS

Part of the nanoparticle research is funded by NSF NIRT (CBET-0708172), NSF (EECS − 0901503), NSF (EECS − 0801774), and NIH (1R01EY022111).

■ ABBREVIATIONS

CNPs = cerium oxide nanoparticles
PAA = polyacrylic acid
$PAA_{1.8}$ = polyacrylic acid of 1.8 kg/mol molecular weight
PAA_{100} = polyacrylic acid of 100 kg/mol molecular weight
PAA_{250} = polyacrylic acid of 250 kg/mol molecular weight

■ REFERENCES

(1) Song, X.; Huang, S.; Gong, B.; Meng, R.; Zhang, M.; Yang, Y.; Zhong, Y.; Jiang, N. Synthesis of Γ-Al2o3/Ceo2 Coated Nanoparticles and Dispersion Stability of their Suspension. *Integ. Ferroelectr.* **2013**, *146* (1), 76−87.

(2) Gaynor, J. D.; Karakoti, A. S.; Inerbaev, T.; Sanghavi, S.; Nachimuthu, P.; Shutthanadan, V.; Seal, S.; Thevuthasan, S. Enzyme-Free Detection of Hydrogen Peroxide from Cerium Oxide Nanoparticles Immobilized on Poly(4-Vinylpyridine) Self−Assembled Monolayers. *J. Mater. Chem. B* **2013**, *1*, 3443−3450.

(3) Li, Y.; Fu, Q.; Flytzani-Stephanopoulos, M. Low-Temperature Water-Gas Shift Reaction over Cu-and Ni-Loaded Cerium Oxide Catalysts. *Appl. Catal., B* **2000**, *27* (3), 179−191.

(4) Korsvik, C.; Patil, S.; Seal, S.; Self, W. T. Superoxide Dismutase Mimetic Properties Exhibited by Vacancy Engineered Ceria Nanoparticles. *Chem. Commun.* **2007**, *10*, 1056−1058.
(5) Heckert, E. G.; Karakoti, A. S.; Seal, S.; Self, W. T. The Role of Cerium Redox State in the Sod Mimetic Activity of Nanoceria. *Biomaterials* **2008**, *29* (18), 2705−2709.
(6) Pirmohamed, T.; Dowding, J. M.; Singh, S.; Wasserman, B.; Heckert, E.; Karakoti, A. S.; King, J. E.; Seal, S.; Self, W. T. Nanoceria Exhibit Redox State-Dependent Catalase Mimetic Activity. *Chem. Commun. (Cambridge, U. K.)* **2010**, *46* (16), 2736−2738.
(7) Wei, H.; Wang, E. Nanomaterials with Enzyme-like Characteristics (Nanozymes): Next-Generation Artificial Enzymes. *Chem. Soc. Rev.* **2013**, *42*, 6060−6093.
(8) Das, S.; Singh, S.; Dowding, J. M.; Oommen, S.; Kumar, A.; Sayle, T. X.; Saraf, S.; Patra, C. R.; Vlahakis, N. E.; Sayle, D. C. The Induction of Angiogenesis by Cerium Oxide Nanoparticles through the Modulation of Oxygen in Intracellular Environments. *Biomaterials* **2012**, *33*, 7746−7755.
(9) Karakoti, A.; Singh, S.; Dowding, J. M.; Seal, S.; Self, W. T. Redox-Active Radical Scavenging Nanomaterials. *Chem. Soc. Rev.* **2010**, *39* (11), 4422−4432.
(10) Dowding, J. M.; Seal, S.; Self, W. T. Cerium Oxide Nanoparticles Accelerate the Decay of Peroxynitrite (ONOO−). *Drug Delivery Transl. Res.* **2013**, 1−5.
(11) Das, S.; Dowding, J. M.; Klump, K. E.; Mcginnis, J. F.; Self, W.; Seal, S. Cerium Oxide Nanoparticles: Applications and Prospects in Nanomedicine. *Nanomedicine* **2013**, *8* (9), 1483−1508.
(12) Tarnuzzer, R. W.; Colon, J.; Patil, S.; Seal, S. Vacancy Engineered Ceria Nanostructures For Protection from Radiation-Induced Cellular Damage. *Nano Lett.* **2005**, *5* (12), 2573−2577.
(13) Wason, M. S.; Colon, J.; Das, S.; Seal, S.; Turkson, J.; Zhao, J.; Baker, C. H. Sensitization of Pancreatic Cancer Cells to Radiation by Cerium Oxide Nanoparticle-Induced ROS Production. *Nanomed.: Nanotechnol., Biol. Med.* **2013**, *9*, 558−569.
(14) Madero-Visbal, R. A.; Alvarado, B. E.; Colon, J. F.; Baker, C. H.; Wason, M. S.; Isley, B.; Seal, S.; Lee, C. M.; Das, S.; Mañon, R. Harnessing Nanoparticles to Improve Toxicity after Head and Neck Radiation. *Nanomed.: Nanotechnol., Biol. Med.* **2012**, *8* (7), 1223−1231.
(15) Colon, J.; Herrera, L.; Smith, J.; Patil, S.; Komanski, C.; Kupelian, P.; Seal, S.; Jenkins, D. W.; Baker, C. H. Protection from Radiation-Induced Pneumonitis using Cerium Oxide Nanoparticles. *Nanomed.: Nanotechnol., Biol. Med.* **2009**, *5* (2), 225−231.
(16) Chen, J.; Patil, S.; Seal, S.; Mcginnis, J. F. Rare Earth Nanoparticles Prevent Retinal Degeneration Induced by Intracellular Peroxides. *Nat. Nanotechnol.* **2006**, *1* (2), 142−150.
(17) Das, M.; Patil, S.; Bhargava, N.; Kang, J.-F.; Riedel, L. M.; Seal, S.; Hickman, J. J. Auto-Catalytic Ceria Nanoparticles offer Neuroprotection to Adult Rat Spinal Cord Neurons. *Biomaterials* **2007**, *28* (10), 1918−1925.
(18) Chigurupati, S.; Mughal, M. R.; Okun, E.; Das, S.; Kumar, A.; Mccaffery, M.; Seal, S.; Mattson, M. P. Effects of Cerium Oxide Nanoparticles on the Growth of Keratinocytes, Fibroblasts and Vascular Endothelial Cells in Cutaneous Wound Healing. *Biomaterials* **2013**, *34*, 2194−2201.
(19) Hirst, S. M.; Karakoti, A. S.; Tyler, R. D.; Sriranganathan, N.; Seal, S.; Reilly, C. M. Anti Inflammatory Properties of Cerium Oxide Nanoparticles. *Small* **2009**, *5* (24), 2848−2856.
(20) Cimini, A.; D'angelo, B.; Das, S.; Gentile, R.; Benedetti, E.; Singh, V.; Monaco, A. M.; Santucci, S.; Seal, S. Antibody-Conjugated Pegylated Cerium Oxide Nanoparticles for Specific Targeting of Aβ Aggregates Modulate Neuronal Survival Pathways. *Acta Biomater.* **2012**, *8* (6), 2056−2067.
(21) Alili, L.; Sack, M.; Von Montfort, C.; Giri, S.; Das, S.; Carroll, K. S.; Zanger, K.; Seal, S.; Brenneisen, P. Downregulation of Tumor Growth and Invasion by Redox-Active Nanoparticles. *Antioxid. Redox Signaling* **2013**, *19*, 765−778.
(22) Giri, S.; Karakoti, A.; Graham, R. P.; Maguire, J. L.; Reilly, C. M.; Seal, S.; Rattan, R.; Shridhar, V. Nanoceria: A Rare-Earth Nanoparticle as a Novel Anti-Angiogenic Therapeutic Agent in Ovarian Cancer. *PLoS One* **2013**, *8* (1), E54578.
(23) Cai, X.; Sezate, S. A.; Seal, S.; Mcginnis, J. F. Sustained Protection Against Photoreceptor Degeneration in Tubby Mice by Intravitreal Injection of Nanoceria. *Biomaterials* **2012**, *33*, 8771−8781.
(24) Deshpande, S.; Patil, S.; Kuchibhatla, S. V.; Seal, S. Size Dependency Variation in Lattice Parameter and Valency States in Nanocrystalline Cerium Oxide. *Appl. Phys. Lett.* **2005**, *87* (13), 133113.
(25) Karimian, H.; Babaluo, A. Halos Mechanism in Stabilizing of Colloidal Suspensions: Nanoparticle Weight Fraction and pH Effects. *J. Eur. Ceram. Soc.* **2007**, *27* (1), 19−25.
(26) Vincent, A.; Inerbaev, T. M.; Babu, S.; Karakoti, A. S.; Self, W. T.; Masunov, A. E.; Seal, S. Tuning Hydrated Nanoceria Surfaces: Experimental/Theoretical Investigations of Ion Exchange and Implications in Organic and Inorganic Interactions. *Langmuir* **2010**, *26* (10), 7188−7198.
(27) Fresnais, J.; Lavelle, C.; Berret, J.-F. Nanoparticle Aggregation Controlled by Desalting Kinetics. *J. Phys. Chem. C* **2009**, *113* (37), 16371−16379.
(28) Gittins, D. I.; Caruso, F. Tailoring the Polyelectrolyte Coating of Metal Nanoparticles. *J. Phys. Chem. B* **2001**, *105* (29), 6846−6852.
(29) Kirby, G. H.; Harris, D. J.; Li, Q.; Lewis, J. A. Poly(Acrylic Acid)−Poly(Ethylene Oxide) Comb Polymer Effects on $BaTiO_3$ Nanoparticle Suspension Stability. *J. Am. Ceram. Soc.* **2004**, *87* (2), 181−186.
(30) Wang, D.; Nap, R. J.; Lagzi, I. N.; Kowalczyk, B.; Han, S.; Grzybowski, B. A.; Szleifer, I. How and Why Nanoparticle's Curvature Regulates the Apparent pKa of the Coating Ligands. *J. Am. Ceram. Soc.* **2011**, *133* (7), 2192−2197.
(31) Lewis, J. A. Colloidal Processing of Ceramics. *J. Am. Ceram. Soc.* **2000**, *83* (10), 2341−2359.
(32) Safi, M.; Sarrouj, H.; Sandre, O.; Mignet, N.; Berret, J.-F. Interactions Between Sub-10-nm Iron and Cerium Oxide Nanoparticles and 3t3 Fibroblasts: The Role of the Coating and Aggregation State. *Nanotechnology* **2010**, *21* (14), 145103.
(33) Qi, L.; Chapel, J.-P.; Castaing, J.-C.; Fresnais, J.; Berret, J.-F. Stability and Adsorption Properties of Electrostatic Complexes: Design of Hybrid Nanostructures for Coating Applications. *Langmuir* **2007**, *23* (24), 11996−11998.
(34) Karakoti, A. S.; Singh, S.; Kumar, A.; Malinska, M.; Kuchibhatla, S. V.; Wozniak, K.; Self, W. T.; Seal, S. PEGylated Nanoceria as Radical Scavenger with Tunable Redox Chemistry. *J. Am. Chem. Soc.* **2009**, *131* (40), 14144−14145.
(35) Xiong, L.; Yang, T.; Yang, Y.; Xu, C.; Li, F. Long-Term in vivo Biodistribution Imaging and Toxicity of Polyacrylic Acid-Coated Upconversion Nanophosphors. *Biomaterials* **2010**, *31* (27), 7078−7085.
(36) Torrado, S.; Prada, P.; De La Torre, P. M.; Torrado, S. Chitosan-Poly(Acrylic) Acid Polyionic Complex: In Vivo Study to Demonstrate Prolonged Gastric Retention. *Biomaterials* **2004**, *25* (5), 917−923.
(37) Sehgal, A.; Lalatonne, Y.; Berret, J.-F.; Morvan, M. Precipitation-Redispersion of Cerium Oxide Nanoparticles with Poly(Acrylic Acid): Toward Stable Dispersions. *Langmuir* **2005**, *21* (20), 9359−9364.
(38) De Laat, A.; Van Den Heuvel, G. Molecular Weight Fractionation in the Adsorption of Polyacrylic Acid Salts onto $BaTiO_3$. *Colloids Surf., A* **1995**, *98* (1), 53−59.
(39) Phenrat, T.; Liu, Y.; Tilton, R. D.; Lowry, G. V. Adsorbed Polyelectrolyte Coatings decrease Fe(0) Nanoparticle Reactivity with TCE in Water: Conceptual Model and Mechanisms. *Environ. Sci. Technol.* **2009**, *43* (5), 1507−1514.
(40) Surve, M.; Pryamitsyn, V.; Ganesan, V. Nanoparticles in Solutions of Adsorbing Polymers: Pair Interactions, Percolation, and Phase Behavior. *Langmuir* **2006**, *22* (3), 969−981.
(41) Jain, P. K.; Lee, K. S.; El-Sayed, I. H.; El-Sayed, M. A. Calculated Absorption and Scattering Properties of Gold Nanoparticles of Different Size, Shape, and Composition: Applications in Biological

Imaging and Biomedicine. *J. Phys. Chem. B* **2006**, *110* (14), 7238−7248.
(42) Pan, Z.; Campbell, A.; Somasundaran, P. Polyacrylic Acid Adsorption And Conformation In Concentrated Alumina Suspensions. *Colloids Surf., A* **2001**, *191* (1), 71−78.
(43) Qi, L.; Sehgal, A.; Castaing, J.-C.; Chapel, J.-P.; Fresnais, J. M.; Berret, J.-F.; Cousin, F. Redispersible Hybrid Nanopowders: Cerium Oxide Nanoparticle Complexes With Phosphonated-PEG Oligomers. *ACS Nano* **2008**, *2* (5), 879−888.
(44) Viota, J. N. L.; Rudzka, K.; Trueba, A. N.; Torres-Aleman, I.; Delgado, A. N. V. Electrophoretic Characterization of Insulin Growth Factor (Igf-1) Functionalized Magnetic Nanoparticles. *Langmuir* **2011**, *27* (10), 6426−6432.
(45) Phenrat, T.; Saleh, N.; Sirk, K.; Kim, H.-J.; Tilton, R. D.; Lowry, G. V. Stabilization of Aqueous Nanoscale Zerovalent Iron Dispersions by Anionic Polyelectrolytes: Adsorbed Anionic Polyelectrolyte Layer Properties and Their Effect On Aggregation And Sedimentation. *J. Nanopart. Res.* **2008**, *10* (5), 795−814.
(46) Ohshima, H. Electrokinetics of Soft Particles. *Colloid Polym. Sci.* **2007**, *285* (13), 1411−1421.
(47) Chane-Ching, J.-Y. Cerium (IV) Compound. U.S. Patent 5,344,588, September 1994.
(48) Chen, H.; Wei, W.-C. J.; Hsu, K.-C.; Chen, C. Adsorption of PAA on the Al_2O_3 Surface. *J. Am. Chem. Soc.* **2007**, *90* (6), 1709−1716.
(49) Pedersen, H. G.; Bergström, L. Forces Measured between Zirconia Surfaces in Poly(Acrylic Acid) Solutions. *J. Am. Chem. Soc.* **1999**, *82* (5), 1137−1145.
(50) Kumar, A.; Babu, S.; Karakoti, A. S.; Schulte, A.; Seal, S. Luminescence Properties of Europium-Doped Cerium Oxide Nanoparticles: Role of Vacancy and Oxidation States. *Langmuir* **2009**, *25* (18), 10998−11007.
(51) Eck, D.; Helm, C. A.; Wagner, N. J.; Vaynberg, K. A. Plasmon Resonance Measurements of the Adsorption and Adsorption Kinetics of a Biopolymer onto Gold Nanocolloids. *Langmuir* **2001**, *17* (4), 957−960.
(52) Liu, Y. Some Consideration on the Langmuir Isotherm Equation. *Colloids Surf., A* **2006**, *274* (1), 34−36.